Computation of Temperature and Stress in the HDR Pressure Vessel in Presence of Mixing Effects in the Cold Leg and Mantle Downcomer

R. W. Wanner, M. Schmid, O. Mercier
Paul Scherrer Institute, Würenlingen, Switzerland
G. E. Neubrech, E. Hansjosten
Kernforschungszentrum Karlsruhe GmbH, Karlsruhe, FRG

INTRODUCTION

The material properties and actual in-service stress levels should be known fairly accurately in order to be able to warrant the tolerance gap between actual loading and load carrying capacity of a nuclear reactor pressure vessel (PV) during its scheduled lifetime. The cold leg and the PV nozzle are highly stressed during cold water feed. Within the Hot Steam Reactor Safety Program the loading of the cold leg and of the PV was investigated in almost full-scale experiments (experiment group TEMB, Schygulla 1986) during a high-pressure feeding from the cold leg. The water temperature was measured at several places in the mantel downcomer and surface temperature and strain on the inside and outside faces of the PV. At one place directly under the TEMB nozzle (Figure 1) also the temperatures at various depths through the wall were recorded. The recorded values deviated considerably from the magnitudes that are to be expected if it is assumed that the cooling is rotationally symmetric and the fluid temperature is the one from the center of the drop shaped cooling zone below the TEMB nozzle. In the circumferential direction the measured strains are significantly lower if the thermal loading is applied locally only ; the opposite obtains in the axial direction. (Neubrech 1987). Extensive post calculation for temperature and strains were performed, where results of 1D and 2D finite element (FE) calculations should be compared with results of 3D FE calculations and the experimental data. In an axisymmetric calculation on a "1D" model (Geiss 1985) the axial and circumferential strains are equal and not conservative with respect to the axial direction. In a 2D calculation (Siebler 1987) excellent agreement was found in azimutal direction but axial strains were significant overestimated. Finally for the 3D calculations which are presented in this paper generally a good agreement was found with measured temperature and strains, but substantial deviations were found close to the TEMB nozzle corner. The main effort for the 3D FE calculation was to define appropriate thermal boundary conditions (BC), to which the resulting computed strains seem to be very sensitive. Therefore additional 1D and 2D calculations were performed, using the thermal BC of the 3D calculations.

TEST FACILITY AND TEMB EXPERIMENT T32.41

A simplified cross section of the PV with the attached TEMB nozzle and cold leg is shown in Figure 1 . The PV and TEMB-nozzle inside are covered by a cladding (in the mean about 7mm thick) of austenitic steel. The experiment T32.41 started from steady state conditions with a uniform temperature of 300 °C of the PV and of the fluid and an internal pressure of 110 bar. A total of 2.6 tons of cold water with a temperature of 16 °C was continuously injected with high pressure in the cold leg during 30 minutes. From the corner of the TEMB nozzle the cold water was pulled down in the downcomer by gravity, thus a drop shaped cooling area developed.

NUMERICAL CALCULATIONS OF TEMPERATURE AND STRAINS

The 3D finite element model (Figure 2) has a crossection net of 90 degrees and a height of 7000 mm. The height above the nozzle is larger than for the real structure but should compensate some of the missing endcap stiffness. However, both temperature and stress analysis showed that this height has a minor influence on the results, since local effects dominate. The model topology is defined by only 490 elements and 2640 nodes which yields a coarse mesh. However the expected large temperature and stress gradients through the wall thickness and in azimutal direction below the nozzle are considered by the mesh refinement (Figure 3.). The 2D model (Figure 4) has a crossection net of 180 degrees, and corresponds to the one used in earlier calculations (Siebler 1987). For the 1D model a prismatic bar is cut out in radial direction from the PV. Zero heat flux and displacement perpendicular to the sections of all models is assumed. The material property sets (Table 1) are identical to the sets used in earlier calculations (Siebler 1987). The main difficulty

	base material	cladding	units
specific heat per volume	4.3	4.3	J/(mm^3 K)
thermal conductivity	4.2 10^{-2}	1.7 10^{-2}	J/(s mm K)
Youngs modulus	190000	190000	N/mm^2
Poisson ratio	.3	.3	
coefficent of thermal expansion	18.4 10^{-6}	14.8 10^{-6}	1/K

Table 1: Material properties.

for the 3D calculation is to define appropriate thermal BC. For a zone of 4000 mm height and approximately 25 degrees in azimutal direction the fluid temperature at the inside of the PV wall may be calculated from

$$T(x,y) \;=\; T_\infty - \Big(A_1 + A_2 \cdot \exp\Big(A_3 \cdot y^{A_4}\Big)\Big) \cdot \exp\{-x^2/\Big(A_5 + A_6 \cdot \exp\left(A_7 \cdot y\right)\Big)\}, \qquad (1)$$

where $x = 1480 \cdot (\varphi_{RDB} - 270°) \cdot \pi/180$ and $y = 8760 - Z_{RDB}$. The coefficients A_i (i=1,7) for this equation are calculated from the fluid temperature measurements in the downcomer (Figure 5) by a time independent procedure. Thus a smooth temperature distribution results from this Equation for a moment as shown in Figure 6 for a time 120 seconds after start of cooling. In a second step the strongly oscillatory behaviour of the coefficients A_i with time is reduced by fitting piecewice polynomials of second order to these curves. The resulting time dependent temperature distribution for a line in circumferential direction at the inside of the PV wall is shown in Figure 7. Equation (1) is only valid for zone A in Figure 8. In the zone D and F the values from the border of zone A are extrapolated in vertical respectively horizontal direction. In zone B the value of the bottom mantleline at the nozzle corner is used. For the zones C and E the temperature measured above the nozzle is used. A parameter study (Siebler 1987) showed that a convection coefficient of 5000 W/(m^2) yields good agreement for calculated and measured wall temperatures. This finding was verified by the 3D calculations. Using a smaller convection coefficient outside the zone below the nozzle corner did barely affect the results. For the 3D calculations generally good agreement compared to the measured temperatures and strains was found (Wanner 1989). Only in a zone below the TEMB nozzle corner deviations of about 20 % were found. This may be explained by the sensitivity of the results to the definition of the environment (fluid) temperature, which was not recorded during the experiment in this zone. Temperatures and strains are compared for 2 positions 410 mm (Figure 9 a,b,c) and 110 mm (Figure 9 d,e,f) below the TEMB nozzle corner. As mentioned above, calculated wall temperatures do not meet measured temperatures very well close to the nozzle corner (Figure 9 d). The wire strain gages were built with the same coefficient of thermal expansion as the surface (cladding) material, therefore the contribution of free thermal expansion could be subtracted from the total strains using a dummy strain gage and an electronic

circuit. For the 1D calculations the total strains for the axial and azimutal directions are 0 but the measured strains are $\Delta T \alpha_T$, where ΔT is the difference from the reference temperature (which was 300 °C for our calculations) and α_T is the coefficient of thermal expansion. The same holds for the axial strains in the 2D calculations since plane strain was assumed. The circumferential strains were significantly overestimated by the 1D calculation. The circumferential strains were larger for the 3D calculations than for the 2D calculations but the deviation from the measured values is smaller than .2 °/₀₀. Finaly all calculated strains are conservative with respect to the measured values. The 1D and 2D calculations differ if the temperature difference from the reference temperature is different. The substantial overestimation found in earlier 2D calculations (Siebler 1987) is due to the assumed simplified fluid temperature distribution. The nonconservative axial strains found in an earlier "1D" calculation (Geiss 1985) may only be explained by the very different BC.

CONCLUSIONS

For two positions (110 and 410 mm) below the lower corner of the TEMB-nozzle PV intersection, results of 1D, 2D and 3D temperature and strain calculations were compared to measured data.

- The large deviations (2D) and nonconservative results ("1D") found in earlier strain calculations may be explained by the different thermal BC ("1D",2D) and mechanical BC ("1D").
- The 3D FE calculations performed with the thermal BC defined above yielded slightly conservative results compared to the experimental data.
- The difference found between the improved 2D and the 3D calculations with respect to the experimental data would not justify the performing of expensive 3D calculations.
- The improved 1D calculations with fixed displacements in axial and circumferential direction also yield conservative strains.
- The computed strains are very sensitive to the variation of environment temperature conditions, but a uniform convection coefficient might be used.
- Stress intensity calculations may be performed, using stress distributions from 2D calculations and unit stress intensity factors of 3D calculations. The wall thickness should be varied up to the values for a pressurized water reactor (approximately 250 mm).

REFERENCES

Geiss, M. (1985). Berechnung der RDB-Wandbeanspruchung bei der Versuchsgruppe T32. Battelle Institut, Frankfurt, FRG PHDR-Arbeitsberichte 2.219/86, 2.220/86.

Neubrech, G. E., Görner, F., Kordisch, H. and Siebler, T. (1987). Temperature, strains and crack behavior during local thermal shock tests on the RPV-cylinder of the HDR. Transactions of the 9th International SMIRT conference, Vol. G, pp. 325-336.

Siebler, T. and Stamm, H. (1987). Nach- und Auslegungsrechnungen für die Langzeitkühlversuche an der HDR-Zylinderwand. Universität Karlsruhe. Institut für Zuverlässigkeit und Schadenskunde im Maschinenbau. PHDR-Arbeitsbericht 2.256/87.

Wanner, R. W., Schmid, M., Neubrech, G. E. and Hansjosten, E. (1989). TEMB: Temperatur und Spannungsberechnungen mit einem 3D Finite Elemente Modell. Paul Scherrer Institute, Switzerland, PHDR-Arbeitsbericht to be published.

Schygulla, U. and Wolf, L. (1986). Untersuchungen von Mischungseffekten im Kaltstrang und Ringraum der HDR-Anlage, Quick-Look-Report Versuchsgruppe TEMB Versuche: T32.11-91. Kernforschungszentrum Karlsruhe, PHDR Technischer Fachbericht Nr. 63-86.

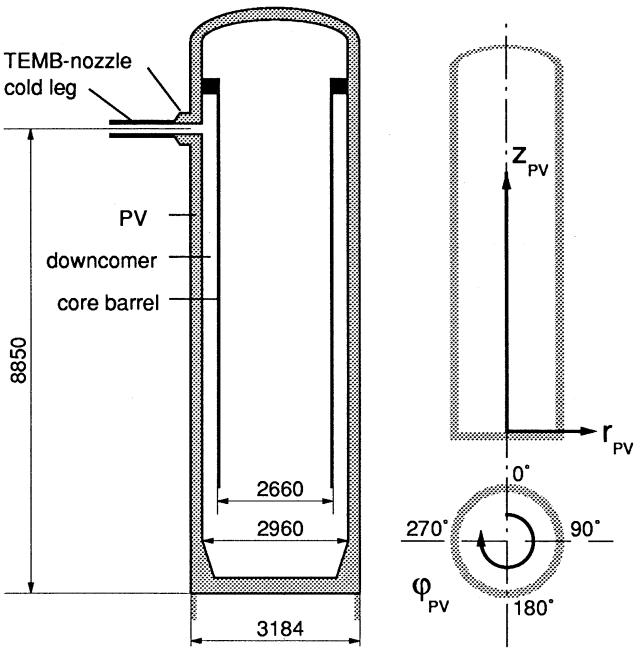

Figure 1: Test facility for the TEMB experiments and PV coordinate system.

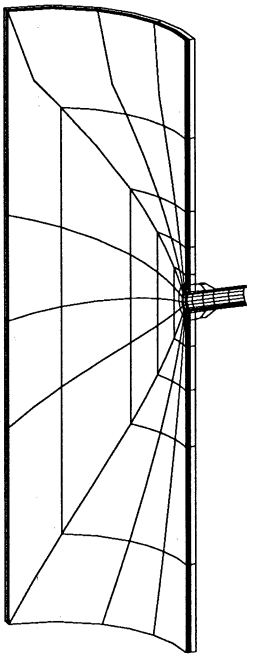

Figure 2: 3D Finite element mesh of the PV.

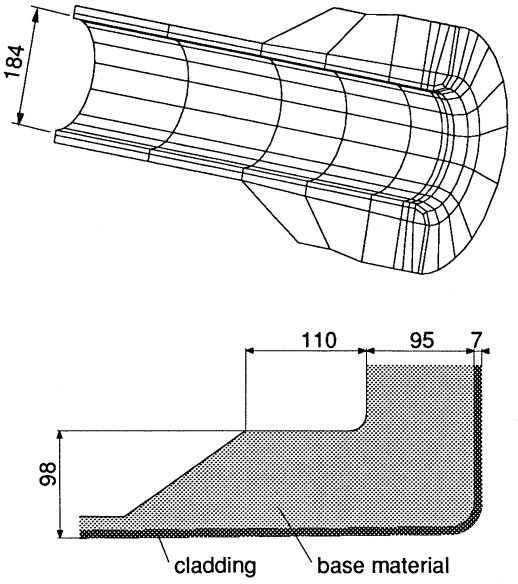

Figure 3: TEMB nozzle geometry and finite element mesh.

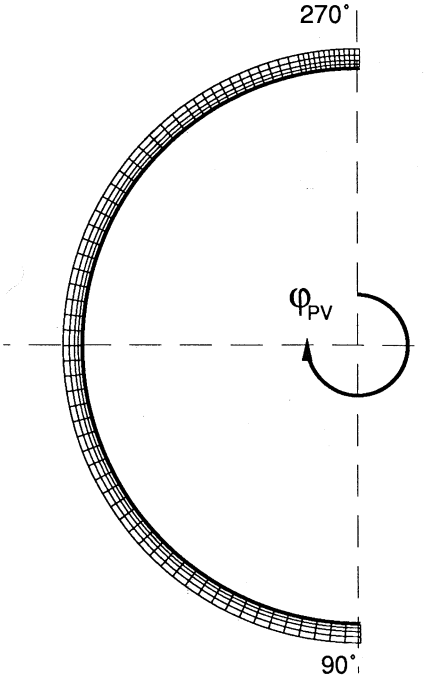

Figure 4: 2D finite element mesh of the PV crossection perpendicular to the axis of revolution.

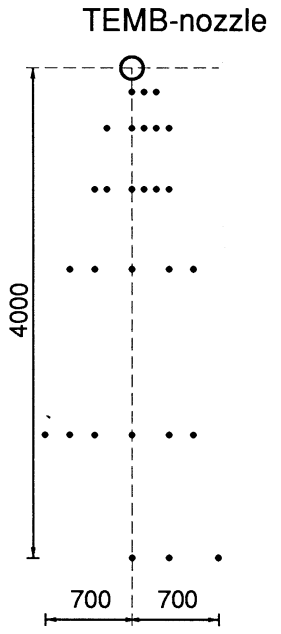

Figure 5: Locations for fluid temperature measurement (filled circles).

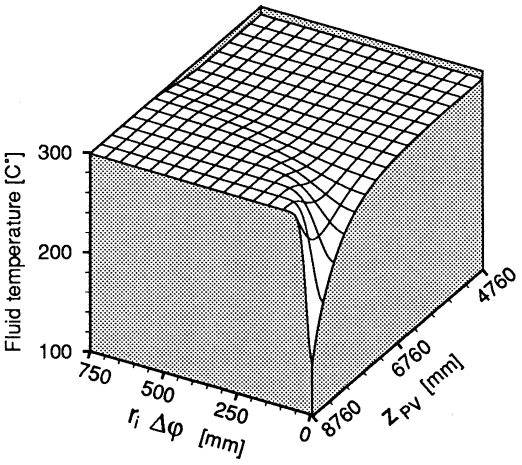

r_i = 1480 mm
$\Delta\varphi = (\varphi_{PV}\text{-}270)\pi/180$

Figure 6: Fluid temperature distribution in a rectangular zone on the PV inside wall below the TEMB nozzle.

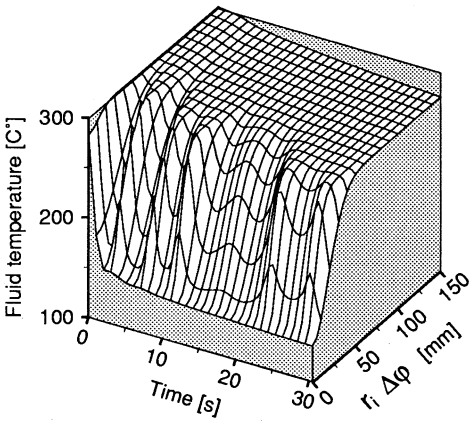

r_i = 1480 mm
$\Delta\varphi = (\varphi_{PV}\text{-}270)\pi/180$

Figure 7: Time dependent fluid temperature distribution on a circumferential line (z_{PV} = 8670) of the PV inside wall below the TEMB-nozzle.

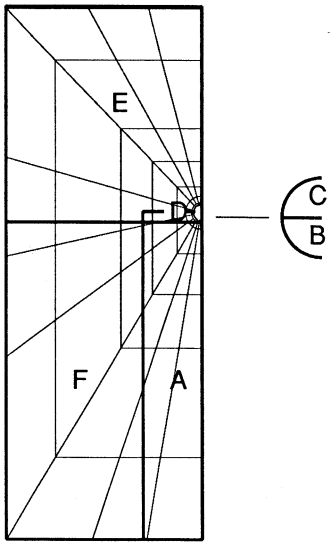

Figure 8: Inside PV wall surface zones for the definition of thermal boundary conditions.

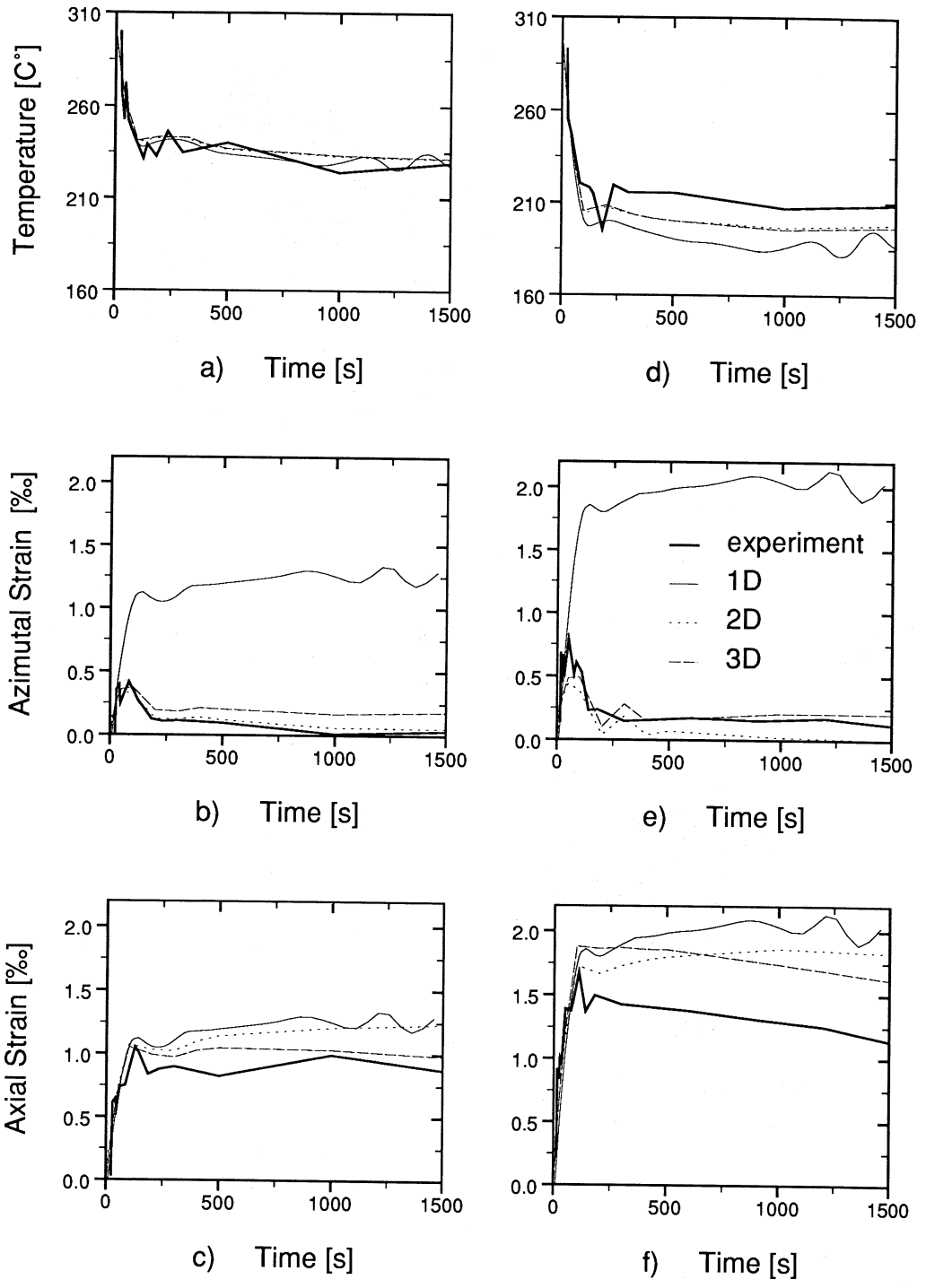

Figure 9: Improved 1D, 2D and 3D calculations compared to measured data, for the positions 410 mm (a,b,c) and 110 mm (d,e,f) below the TEMB nozzle corner.